ChemComm

COMMUNICATION

View Article Online
View Journal

Cite this: DOI: 10.1039/d1cc06682j

Received 28th November 2021,
Accepted 14th December 2021

DOI: 10.1039/d1cc06682j

rsc.li/chemcomm

Encapsulation of atomically dispersed Pt clusters in porous TiO_2 for semi-hydrogenation of phenylacetylene†

Huibin Wu,[ab] Xinchun Yang,[ab] Shichao Zhao,[a] Liming Zhai,[ab] Guofu Wang,[a] Bin Zhang *[ab] and Yong Qin [ab]

The synthesis of atomically dispersed metal clusters with strong interaction with the support is attractive for the design of high-efficiency catalysts. Here, we report a multilayered catalyst (1.91%Pt@TiO_2), in which atomically dispersed Pt clusters are encapsulated in the porous TiO_2. As a result, 1.91%Pt@TiO_2 exhibited high activity, selectivity (92.9%), and excellent stability in the semi-hydrogenation of phenylacetylene.

The full dispersion of the metal on the support is crucial for advanced catalysis and has been realized on single-atom catalysts (SACs) and atomically dispersed metal cluster catalysts and attracted widespread attention in the last decade.[1,2] The presence of atomic discrete metal centers endows SACs with full atomic utilization efficiency but limits loading, stability, and applications.[3] In contrast, atomically dispersed metal cluster catalysts provide multiple metal atoms on the support and exhibit increased stability and activity compared to SACs.[4] For instance, the TOF of Au aggregates of 5–10 atoms is the same order of enzymes and higher than that of isolated Au atoms in the aerobic oxidation of thiophenol, but the Au clusters finally aggregate into larger and inactive nanoparticles.[5] Strong metal–support interaction (SMSI) facilitates the stabilization of the clusters. Atomic-layer Au clusters on α-MoC with SMSI can realize an ultralow-temperature water–gas shift reaction with higher activity than SACs and support metal nanoparticle catalysts.[6] However, the aggregation and leaching of metal atoms during the reaction is still unavoidable. It remains a challenge to simultaneously synthesize atomically dispersed metal cluster catalysts with numerous active metal sites and superior stability.

Atomic layer deposition (ALD) is a cyclic process that relies on two sequential self-limiting surface reactions on the substrate at the atomic level.[7–9] This unique character makes ALD possible to bottom–up construct catalysts precisely. Herein, we report a general strategy for synthesizing multilayered catalysts to encapsulate atomically dispersed metal clusters in the porous metal oxide using template-assisted ALD. Typically, multilayered catalyst 1.91%Pt@TiO_2 was synthesized, and atomically dispersed Pt clusters were encapsulated in the porous TiO_2. Porous TiO_2 supported Pt clusters with a bigger size were also synthesized by ALD to reveal the effect of Pt–TiO_2 interaction. 1.91%Pt@TiO_2 exhibited high selectivity and excellent stability in the semi-hydrogenation of phenylacetylene, affording styrene selectivity as high as 92.9% with a phenylacetylene conversion of 93.4%. Compared to the supported Pt cluster catalysts with bigger Pt clusters, the high selectivity of 1.91%Pt@TiO_2 is attributed to the weak styrene adsorption and high activation energy of styrene hydrogenation on the electron-deficient Pt clusters.

The multilayered catalyst 1.91%Pt@TiO_2 with a Pt loading of 1.91 wt% was synthesized by repeated depositions of the TiO_2 layer (A) and Pt layer (B) on the carbon nanofibers (CNFs), followed by calcination at 450 °C in the air (Scheme 1). The ALD cycle numbers were 30 for the deposition of the TiO_2 layer and

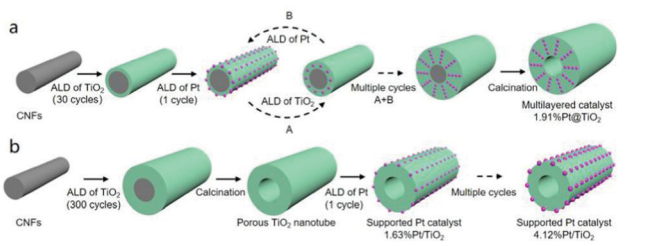

Scheme 1 Schematic of the synthesis process of the multilayered catalyst (1.91%Pt@TiO_2) (a), and supported Pt catalysts (1.63%Pt/TiO_2 and 4.12%Pt/TiO_2) (b).

[a] State Key Laboratory of Coal Conversion, Institute of Coal Chemistry, Chinese Academy of Sciences, Taiyuan 030001, China. E-mail: zhangbin2009@sxicc.ac.cn
[b] Center of Materials Science and Optoelectronics Engineering, University of Chinese Academy of Sciences, Beijing 100049, China

† Electronic supplementary information (ESI) available. See DOI: 10.1039/d1cc06682j

1 for the deposition of the Pt layer. The repeated times of the TiO_2 and Pt layer were 10, and one more TiO_2 layer was deposited to ensure the overall overcoating. When the TiO_2 ALD cycle numbers increased to 100 and repeated times of the A + B sequence reduced to 5, 0.57%Pt@TiO_2 with a Pt loading of 0.57 wt% was obtained. The supported Pt/TiO_2 catalysts were also synthesized for comparison. First, the porous TiO_2 nanotube support was synthesized by depositing 300 cycles of TiO_2 on CNFs, followed by calcination in air at 450 °C. Then, 1.63%Pt/TiO_2 and 4.12%Pt/TiO_2 were synthesized by depositing one cycle and three cycles of Pt on porous TiO_2 nanotubes, respectively.

Aberration-corrected high angle annular dark-field scanning transmission electron microscopy (HAADF-STEM) measurements were carried out to investigate the morphology of the catalysts. Atomically dispersed Pt clusters with an average size of 0.5 nm are located in the porous TiO_2 nanotubes for 1.91%Pt@TiO_2 (Fig. 1a and Fig. S1a, ESI†). For 1.63%Pt/TiO_2 (Fig. 1b and Fig. S1c, ESI†) and 4.12%Pt/TiO_2 (Fig. 1c and Fig. S1d, ESI†), Pt clusters are located on the TiO_2 nanotube. The average size of Pt clusters increases from 1.0 nm over 1.63%Pt/TiO_2 to 1.6 nm over 4.12%Pt/TiO_2. Considering the size and location of Pt species, the interaction between Pt and TiO_2 increases in the order 4.12%Pt/TiO_2, 1.63%Pt/TiO_2, and 1.91%Pt@TiO_2.

In order to clarify the electronic structure of the Pt catalysts, X-ray absorption fine structure (XAFS) spectra tests were performed. No A, B peaks of the Pt foil but only C peak (Fig. 2a) indicate that oxidized Pt species ($Pt^{\delta+}$) dominantly exist in 1.91%Pt@TiO_2.[10] Although the oxidized Pt species are also dominated over 1.63%Pt/TiO_2 and 4.12%Pt/TiO_2, the weak A peak suggests the presence of metallic Pt species. The intensity of the white line decreases in the order: 1.91%Pt@TiO_2 > 1.63%Pt/TiO_2 > 4.12%Pt/TiO_2, implying the valence decrease in the Pt species. Fig. 2b displays the Fourier transforms of the extended X-ray absorption fine structure (EXAFS) spectra of these catalysts. A dominated peak around 1.60 Å is observed for the three catalysts and can be assigned to the Pt–O coordination.[11,12] Since the Pt–Pt bond contribution can be ignored, the Pt–O coordination is assigned to the chemical bonding between Pt and TiO_2. Correspondingly, the Pt–O coordination numbers decrease in the order: 1.91%Pt@TiO_2 (5.0) > 1.63%Pt/TiO_2 (4.5) > 4.12%Pt/TiO_2 (4.1) (Table S1, ESI†). The higher Pt–O coordination number on 1.91%Pt@TiO_2 suggests the higher valence of oxidized Pt species and stronger interaction between Pt and TiO_2 than that on 1.63%Pt/TiO_2 and 4.12%Pt/TiO_2.

In-situ diffuse reflectance infrared Fourier transform spectroscopy (DRIFTS) CO chemisorption measurements were performed to explore the surface structure of the Pt catalysts. For CO adsorption on 1.91%Pt@TiO_2 (Fig. 2c), the dominant peak of 2100 cm^{-1} for linear adsorbed CO and no peak of ~1850 cm^{-1} for bridged-bonded CO indicate that most of the Pt atoms are in high electron deficiency, and no metallic Pt–Pt bonds are formed.[13,14] CO adsorption with a bit of redshift (2095 cm^{-1}) is observed for 1.63%Pt/TiO_2. For 4.12%Pt/TiO_2,

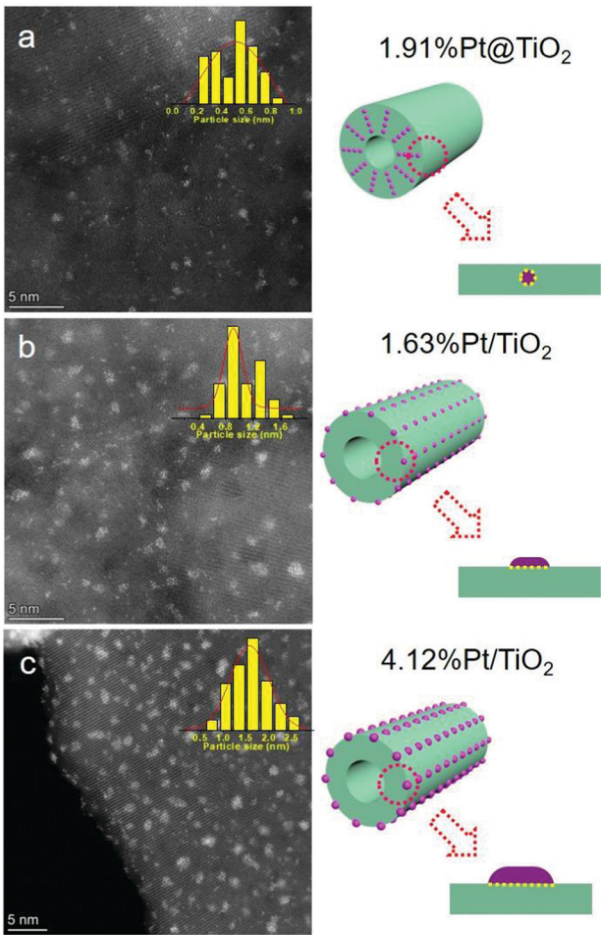

Fig. 1 Aberration-corrected HAADF-STEM images and corresponding interfacial structure of 1.91%Pt@TiO_2 (a), 1.63%Pt/TiO_2 (b) and 4.12%Pt/TiO_2 (c).

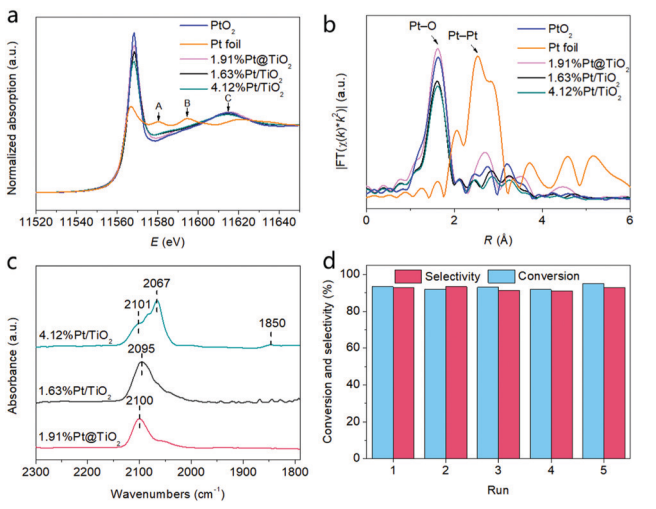

Fig. 2 (a) XANES spectra of different samples as well as the Pt foil and PtO_2 reference at the Pt L_3 edge. (b) The corresponding k^2-weighted Fourier transform spectra in the R space. (c) DRIFTS of CO chemisorption on different samples at 30 °C. (d) Recyclability test of the 1.91%Pt@TiO_2.

Table 1 Tandem reactions of the hydrolysis of ammonia borane (AB) and hydrogenation of phenylacetylene (PA) over different Pt-based catalysts[a]

Entry	Catalyst	Time (min)	TOF[c] (h^{-1})	Conv. (%)	Sel. (%)
1	1.91%Pt@TiO_2	40	657.6	93.4	92.9
2	0.57%Pt@TiO_2	145	—	92.0	92.3
3	1.63%Pt/TiO_2	16	1463.7	92.8	80.7
4	4.12%Pt/TiO_2	6	1875.7	92.0	48.2
5[b]	30TiO_2/Pt/TiO_2	220	232.4	98.0	95.0

[a] Reaction condition: 0.09 mmol of phenylacetylene, 1 mmol of ammonia borane, 10 mg of catalyst, EtOH/H_2O = 10 mL/10 mL, 303 K. [b] Results from the ref. 18, the average size of Pt nanoparticle on 30TiO_2/Pt/TiO_2 is 3.0 nm. [c] TOF is calculated basing the CO chemisorption and the kinetics test at low conversion (<10%).

the dominant linear-bonded CO peak at 2067 cm^{-1} along with a shoulder peak at 2101 cm^{-1} and bridge-bonded CO peak at 1850 cm^{-1} are observed, suggesting the presence of Pt–Pt metallic bonds.

The porosity of the catalysts was determined by nitrogen BET (Brunauer–Emmett–Teller) measurements. 1.91%Pt@TiO_2, 1.63%Pt/TiO_2, and 4.12%Pt/TiO_2 show similar N_2 adsorption–desorption isotherms (Fig. S2a, ESI†), calculated BET surface area (80–90 m^2 g^{-1}) and pore distribution (1.7 nm) (Fig. S2b and Table S2, ESI†). The mesopores are formed from the stress relaxation of amorphous TiO_2 during the phase transition to anatase and the removal of carbon residues during high-temperature treatments.[7,15] With these mesopores, the encapsulated Pt species are accessible to the reactants.

The catalytic performance of the Pt-based catalysts was evaluated in the tandem hydrolysis of ammonia borane (AB) and hydrogenation of phenylacetylene (PA) at 30 °C (Table 1). AB with a high hydrogen storage of 19.6 wt% can quickly release hydrogen and is a non-toxicity hydrogen source for hydrogenation.[16,17] The multilayered catalysts 1.91%Pt@TiO_2 and 0.57%Pt@TiO_2 exhibited a high styrene selectivity of 92% at a high conversion of phenylacetylene. The similar performance of 1.91%Pt@TiO_2 and 0.57%Pt@TiO_2 indicates that the distance between Pt layers and the density of Pt cluster distribution over the multilayered catalyst does not affect the reaction selectivity. In contrast, low styrene selectivity is observed over 4.12%Pt/TiO_2 (48.2%) and 1.63%Pt/TiO_2 (80.7%) due to over-hydrogenation.

We have compared the catalytic performance of different Pt-based catalysts reported in the literature in the hydrogenation of phenylacetylene, and the results are listed in Table 1, Table S3, and Fig. S3 (ESI†). Only a few Pt-based catalysts exhibited a higher selectivity than 90% at high conversion (>90%). For the catalyst with selectivity and conversion higher than 90%, 1.91%Pt@TiO_2 performs the highest TOF. Typically, the TOF of 1.91%Pt@TiO_2 (657.6 h^{-1}) is 2.8-fold of the reported sandwich catalyst 30TiO_2/Pt/TiO_2 (232.4 h^{-1}), in which Pt nanoparticles with a size of 3.0 nm are covered by two porous TiO_2 nanolayers (Fig. S4, ESI†).[18]

The multilayered structure can avoid the aggregation and leaching of Pt atoms during the reaction. The activity and selectivity were well maintained during the five consecutive runs (Fig. 2d). The aberration-corrected HAADF-STEM image of 1.91%Pt@TiO_2 after five consecutive runs is similar to that of the fresh samples (Fig. S5, ESI†), indicating its excellent stability.

X-Ray photoelectron spectroscopy (XPS) was performed to investigate the electronic structure of Pt after the reaction (Fig. 3a). The Pt 4f spectra of the three samples were fitted by three doublets, attributed to the metallic Pt^0 species (71.5 and 74.9 eV), Pt^{2+} species (72.7 and 75.9 eV), and Pt^{4+} species (73.9 and 77.2 eV), respectively (Table S4, ESI†). The ratio of metallic Pt^0 species is 38.7% on 1.63%Pt/TiO_2 and 42.8% on 4.12%Pt/TiO_2. Compared to 4.12%Pt/TiO_2, the slight ratio decrease of metallic Pt^0 species on 1.63%Pt/TiO_2 relates to the formation of more oxidized Pt^{4+} species. On 1.91%Pt@TiO_2, the metallic Pt^0 species decreased to 18.2%, and the oxidized Pt species became the dominant species. Thus, the multilayered structure of 1.91%Pt@TiO_2 maintains Pt species in oxidation states during the reaction.

We have tested the rate of ammonia borane (AB) hydrolysis to hydrogen and the phenylacetylene hydrogenation in hydrogen to reveal the rate-determining step in the tandem reaction (Fig. S6 and Table S5, ESI†). The hydrogen consumption rate of the phenylacetylene hydrogenation is 0.041 mmol h^{-1} using H_2 as a hydrogen source and 0.135 mmol h^{-1} in the tandem reaction, which is obviously lower than the rate of ammonia borane (AB) hydrolysis to hydrogen (2.729 mmol h^{-1}). Thus, the rate-determining step is not the ammonia borane (AB) hydrolysis but the hydrogenation of phenylacetylene.

In general, high selectivity is obtained by suppressing the styrene over-hydrogenation. Reaction kinetics of styrene hydrogenation and styrene adsorption were conducted to reveal the mechanism. A relative higher activation energy (E_a = 54.1 kJ mol^{-1}) is observed over 1.91%Pt@TiO_2 compared to 4.12%Pt/TiO_2 (E_a = 43.9 kJ mol^{-1}) (Fig. 3b). The higher

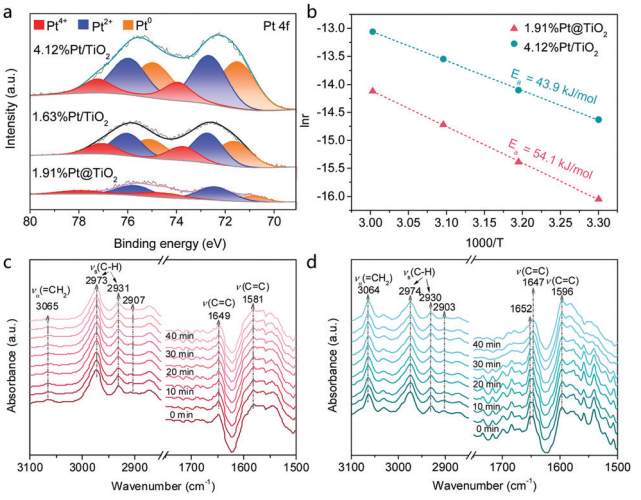

Fig. 3 (a) Pt 4f XPS spectra. (b) Arrhenius plots and the activation energy (E_a) for the tandem hydrolysis of ammonia borane and hydrogenation of styrene over 1.91%Pt@TiO_2 and 4.12%Pt/TiO_2. FT-IR spectra of styrene saturated adsorption on 1.91%Pt@TiO_2 (c) and 4.12%Pt/TiO_2 (d) purged in Ar flow for different times (0–45 min).

E_a indicates that the C=C bond hydrogenation of styrene is kinetically unfavorable over 1.91%Pt@TiO_2. We have further carried out the FT-IR spectroscopy measurements of styrene adsorption on 1.91%Pt@TiO_2 (Fig. 3c) and 4.12%Pt/TiO_2 (Fig. 3d). The typical absorbance bands of styrene, asymmetric stretching vibration of $=CH_2$ bond (ν_a, 3064–3065 cm^{-1}) and C=C bond (1647–1649 cm^{-1}) on the vinyl group,[19] are observed for the two catalysts. The lower intensity of these two peaks on 1.91%Pt@TiO_2 suggests its weaker styrene adsorption than 4.12%Pt/TiO_2. In addition, a new asymmetric stretching vibration of the C=C bond is detected at 1652 cm^{-1} on 4.12%Pt/TiO_2. Since the intensity of the peak at 1652 cm^{-1} decreases with the increase in the purge time in Ar flow, we can consider this to be an active and unstable adsorbed species for further hydrogenation. Thus, we can speculate that the high selectivity on 1.91%Pt@TiO_2 originates from the weak adsorption of the C=C bond and high activation energy for C=C bond hydrogenation.

In summary, atomically dispersed Pt clusters were encapsulated into a multilayered catalyst by ALD. The resulting catalyst 1.91%Pt@TiO_2 exhibited high selectivity towards the semi-hydrogenation of phenylacetylene, affording styrene selectivity as high as 92.9% with a phenylacetylene conversion of 93.4%. The multilayered structure enhances the interaction between atomically dispersed Pt oxide species and TiO_2 and suppresses the formation of metallic Pt species during the reaction. The atomically dispersed Pt oxide species in the multilayered structure exhibit high TOF and selectivity by weakening styrene adsorption and inducing high activation energy of styrene hydrogenation. Besides, 1.91%Pt@TiO_2 possesses excellent stability due to the strong interaction between Pt clusters and TiO_2. The strategy of the bottom–up method by ALD to synthesize the multilayered catalyst is potentially essential for developing highly efficient heterogeneous catalysts.

We acknowledge the financial support from the National Natural Science Foundation of China (21872160, 22072172), National Science Fund for Distinguished Young Scholars (21825204), the National Key R&D Program of China (2017YFA0700101 and 2018YFB1501602), the Youth Innovation Promotion Association CAS (2017204), Natural Science Foundation of Shanxi Province (201901D211591), Youth Training Programme of State Key Laboratory of Coal Conversion (2021BWZ005).

Conflicts of interest

The authors declare no competing financial interest.

Notes and references

1 M. Peng, C. Dong, R. Gao, D. Xiao, H. Liu and D. Ma, *ACS Cent. Sci.*, 2020, **7**, 262–273.
2 S. Mitchell and J. Pérez-Ramírez, *Nat. Rev. Mater.*, 2021, **6**, 969–985.
3 L. Li, X. Chang, X. Lin, Z.-J. Zhao and J. Gong, *Chem. Soc. Rev.*, 2020, **49**, 8156–8178.
4 E. C. Tyo and S. Vajda, *Nat. Nanotechnol.*, 2015, **10**, 577–588.
5 A. Corma, P. Concepcion, M. Boronat, M. J. Sabater, J. Navas, M. J. Yacaman, E. Larios, A. Posadas, M. A. Lopez-Quintela, D. Buceta, E. Mendoza, G. Guilera and A. Mayoral, *Nat. Chem.*, 2013, **5**, 775–781.
6 S. Yao, X. Zhang, W. Zhou, R. Gao, W. Xu, Y. Ye, L. Lin, X. Wen, P. Liu, B. Chen, E. Crumlin, J. Guo, Z. Zuo, W. Li, J. Xie, L. Lu, C. J. Kiely, L. Gu, C. Shi, J. A. Rodriguez and D. Ma, *Science*, 2017, **357**, 389–393.
7 H. Ge, B. Zhang, X. Gu, H. Liang, H. Yang, Z. Gao, J. Wang and Y. Qin, *Angew. Chem., Int. Ed.*, 2016, **55**, 7081–7085.
8 B. Zhang and Y. Qin, *ACS Catal.*, 2018, **8**, 10064–10081.
9 H. Wu, B. Zhang, H. Liang, L. Zhai, G. Wang and Y. Qin, *The Innovation*, 2020, **1**, 100029.
10 A. Munozpaez and D. C. Koningsberger, *J. Phys. Chem.*, 1995, **99**, 4193–4204.
11 X. Cheng, Y. Li, L. Zheng, Y. Yan, Y. Zhang, G. Chen, S. Sun and J. Zhang, *Energy Environ. Sci.*, 2017, **10**, 2450–2458.
12 J. Han, Y. Kim, D. H. K. Jackson, H. Chang, H. W. Kim, J. Lee, J.-R. Kim, Y. Noh, W. B. Kim, K.-Y. Lee and H. J. Kim, *Appl. Catal., B*, 2020, **273**, 119037.
13 C.-T. Kuo, Y. Lu, L. Kovarik, M. Engelhard and A. M. Karim, *ACS Catal.*, 2019, **9**, 11030–11041.
14 J. Li, Q. Guan, H. Wu, W. Liu, Y. Lin, Z. Sun, X. Ye, X. Zheng, H. Pan, J. Zhu, S. Chen, W. Zhang, S. Wei and J. Lu, *J. Am. Chem. Soc.*, 2019, **141**, 14515–14519.
15 S. Karwal, T. Li, A. Yanguas-Gil, C. P. Canlas, Y. Lei, A. U. Mane, J. A. Libera, S. Seifert, R. E. Winans and J. W. Elam, *J. Vac. Sci. Technol., A*, 2018, **36**, 01A103.
16 Q. Sun, N. Wang, T. Zhang, R. Bai, A. Mayoral, P. Zhang, Q. Zhang, O. Terasaki and J. Yu, *Angew. Chem., Int. Ed.*, 2019, **58**, 18570–18576.
17 M. Shen, H. Liu, C. Yu, Z. Yin, M. Muzzio, J. Li, Z. Xi, Y. Yu and S. Sun, *J. Am. Chem. Soc.*, 2018, **140**, 16460–16463.
18 H. Liang, B. Zhang, H. Ge, X. Gu, S. Zhang and Y. Qin, *ACS Catal.*, 2017, **7**, 6567–6572.
19 A. Marchand and J.-P. Quintard, *Spectrochim. Acta, Part A*, 1980, **36**, 941–956.

